Splay and bend disclinations in multidomain vertical-alignment liquid-crystal cells

Jin-Soo Jung[1,2] and Jang-Kun Song[1,*]
[1]*School of Electronic & Electrical Engineering, Sungkyunkwan University, Suwon 440-746, Korea*
[2]*LCD R&D Center, Samsung Display Company, Suwon 446-711, Korea*
(Received 26 April 2012; published 6 July 2012)

We investigated the domain boundary formations in multidomain vertical-alignment nematic liquid-crystal (VA LC) cells. There are two types of domain boundaries in multidomain VA cells, splay and bend type domains, the boundaries of which are dominated by the splay and bend deformations, respectively. Each type could be achieved by either the single-4-domain pair or the 2-2-domain pair of two substrates and have four different domain arrangements. We demonstrated that the disclination width of the splay type domain is about 50% wider than that of the bend type domain even when the splay and bend elastic constants are the same. The difference is so large that it cannot be compensated for by adjusting the elastic constants of the LCs within realistic material parameter ranges. The mechanism of the phenomenon was investigated by disassembling the elastic deformation strains into each component and analyzing them individually. The large difference was revealed to arise from the different twist deformation strains near the surface, which is significantly larger in the bend type than in the splay type. We also suggest an asymmetric pretilt structure, which dramatically reduces the domain boundary width. However, simple adoption of a large pretilt angle is not effective for reducing the width. The experimental results obtained in real LC display panels qualitatively agree well with the simulation results.

DOI: 10.1103/PhysRevE.86.011702 PACS number(s): 61.30.Gd, 61.30.Jf, 61.72.Lk

I. INTRODUCTION

A multidomain structure is common in vertical-alignment liquid-crystal displays (VA LCDs). In early type VA LCDs, the multidomain was produced by a patterned electrode or the morphological protrusion on two substrates [1,2] where the two neighboring domains separated by a pattern or protrusion had an azimuthal angle difference of 180° from each other. In 2004, polymer-stabilized VA (PSVA) was introduced [3], and it was commercialized around 2007. In PSVA, the pixel electrode has a quadrant fish-bone shape forming four domains, whereas, the other side substrate does not have any domain dividing means, as shown in Figs. 1(a-i) and 1(b-i), which is referred to as a (1×4) type domain implying that the upper substrate has a single domain and the bottom substrate has four domains. Photoinduced multidomain LC alignment was suggested in 1996 by Schadt *et al*. [4], and recently, it was first adopted in a commercial VA LCD by SHARP Co., Ltd., Japan in 2010 [5]. In the photoalignment VA, two slanted UV irradiations are exposed on the photosensitive alignment layer coated on each substrate, making two different surface areas [6]. The LC layer, which is cross sandwiched by the two UV-exposed substrates, forms a 4-domain vertical alignment as indicated in Figs. 1(a-ii) and 1(b-ii), which is referred to as (2×2) type domains. Miyachi *et al*. claimed that the adoption of the photoalignment method improved the optical transmittance of the device by more than 20%, which mostly resulted from the reduced total length of domain boundaries [5]. The neighboring two domains in the (1×4) and (2×2) type domains have an azimuthal angle difference of 90°, which is half the azimuthal deformation of the earlier type VA modes. Hence, it has narrower domain boundaries as well. However, the domain boundary is still a main cause of the optical losses. Usually, the domain boundary is seen as a roughly 10 μm wide dark line in the actual multidomain VA cells.

In a perfect vertical alignment LC cell, the alignment layer is isotropic azimuthally, and therefore, the surface does not have azimuthal anchoring for the LC alignment. Slanted UV or ion-beam irradiation on the surface induces a small pretilted LC alignment from normal to the surface [5,7], and the surface can determine the azimuthal tilting direction of LCs based on the application of fields. Nonetheless, the control ability of the azimuthal directors by the surface with the pretilt angle is so weak that the width of the boundaries is quite large compared to planar multidomain LC cells [8,9]. Hence, a disclination width larger than 40 μm has been reported when the surface anchoring was not strong enough [7] and Schlieren texture [10] or peculiar texture [11] was observed due to the weak anchoring. In planar multidomain cells, the position of the disclination line can be unstable [8].

Two types of domain boundaries can be formed depending on the UV irradiation direction: a splay deformation and a bend deformation of LC directors in the boundaries as shown in Figs. 1(a) and 1(b), respectively. Usually, the bend elastic constant (K_{33}) is larger than the splay elastic constant (K_{11}) due to the rod-shaped molecular structure of the LCs [12]. Hence, the boundary width of the splay disclination in Fig. 1(a) is expected to be thinner than the width of the bend disclination in Fig. 1(b). However, interestingly, we obtained opposite results in both experiments and simulations, which was the initial motivation of this paper.

In this paper, we investigated the cause and mechanism influencing the width of the domain boundary in multidomain VA cells. In particular, the difference between the splay and the bend disclination lines was examined in detail by using computer simulations. We examined the optimum conditions to minimize the boundary width in order to reduce optical losses. We also introduce a new and effective way to reduce the boundary width further in multidomain VA cells. The method involves the asymmetric pretilt angle near the boundaries,

*jk.song@skku.edu

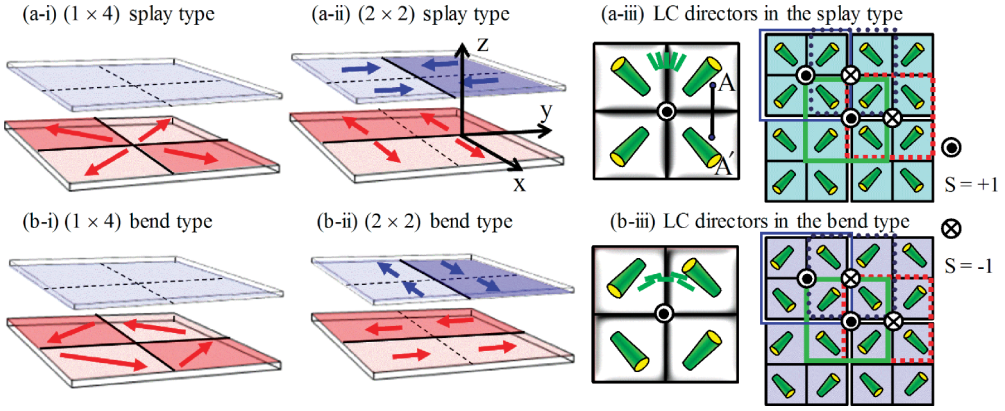

FIG. 1. (Color online) Classification of multidomain structures in the multidomain VA LCDs where (a) represents splay type domains and (b) corresponds to bend type domains. (a-i) and (b-i) are for the (1 × 4) type domain formation, and (a-ii) and (b-ii) are for the (2 × 2) type domain formation. (a-iii) and (b-iii) are the illustrations of the middle-layer LC directors.

which effectively reduces the pretilt angle, and the effect of the suggested method was confirmed by experimental results in a real photoalignment VA cell.

II. BACKGROUND AND SIMULATION OF THE DOMAIN BOUNDARY WIDTH

A. Classification of four domain structures

In the photoalignment VA LC cell, LC pretilt angles (θ_0) of about $1^\circ - 3^\circ$ from normal to substrates are achieved by oblique UV irradiation. As explained in the Introduction section, the four domains with minimal distortion between neighboring domains can be obtained by using either the (1 × 4) process [see Figs. 1(a-i) and 1(b-i)] or the (2 × 2) process [see Figs. 1(a-ii) and 1(b-ii)]. Usually, the photoalignment method adopts the (2 × 2) process. The arrows on the substrates in Figs. 1(a-i), 1(a-ii), 1(b-i) and 1(b-ii) indicate the azimuthal direction of the pretilted director. The rods in Figs. 1(a-iii) and (b-iii) indicate the average tilting direction of molecules in the middle layer of the LCs under the application of electric fields. The LC directors splay out from the center of the four domains in Fig. 1(a), and these rotate around the center in Fig. 1(b). Hence, the domain boundaries in Fig. 1(a) have mostly the splay deformation (which will be called "splay type" domains hereafter), whereas, those in Fig. 1(b) have mostly the bend deformation (which will be called "bend type" domains hereafter).

Meanwhile, the translational multiplication of the four domains produces four types of singular point defects (called "nuclei" or "noyaux") for each type, two of which have a defect strength S of $+1$ and the other two of which have an S of -1 [see the right-side images in Figs. 1(a-iii) and 1(b-iii) [12]. For the splay type domains, the two $+1$ point defects (nuclei) appear in the centers of the diverging and converging four domains (solid square boxes), and the two -1 point defects (nuclei) appear in the centers of the other types of domains (dotted square boxes). The two sets of four domains around the $+1$ point defects (nuclei) are identical due to the flipping symmetry of the cell. The other two sets of four domains around the -1 point defects (nuclei) are also identical. The same analysis is applicable for the bend type domains as well. Thus, for both the splay type and the bend type domains, four different types of domain arrangements are possible. All of the splay type domains have domain boundaries, which are dominant with the splay deformation, and all of the bend type domains have domain boundaries, which are dominant with the bend deformation. Hence, it is expected that the domain boundary width may be dominantly determined by K_{11} for the splay type domains and by K_{33} for the bend type domains. In order to verify this, we carried out simulations, as described in the next section.

B. Simulation of the domain boundary width

The static director distribution can be determined by considering both the elastic free energy and the electric free energy of the LC layer. The elastic free energy density of the deformed LC alignment can be expressed as follows [13,14]:

$$f_{\text{elastic}} = \tfrac{1}{2}K_{11}(\text{div}\ \mathbf{n})^2 + \tfrac{1}{2}K_{22}(\mathbf{n}\cdot\text{curl}\ \mathbf{n})^2 + \tfrac{1}{2}K_{33}(\mathbf{n}\times\text{curl}\ \mathbf{n})^2. \quad (1)$$

Here, (div $\mathbf{n}$), ($\mathbf{n}\cdot$ curl $\mathbf{n}$), and ($\mathbf{n}\times$ curl $\mathbf{n}$) are the splay, twist, and bend deformation strains of the director $\mathbf{n}$, respectively, and K_{11}, K_{22}, and K_{33} are the respective elastic constants.

The electric free energy in nematic LCs, which do not have a spontaneous polarization, is governed by the dielectric anisotropy ($\Delta\varepsilon$), and the electric free energy density under application of the electric field (E) across the cell can be simply expressed as

$$f_{\text{electric}} = \tfrac{1}{2}\varepsilon_0\Delta\varepsilon\ \sin^2\theta E^2, \quad (2)$$

where θ is the polar angle of the director from normal to the surface. In the VA LC cell, $\Delta\varepsilon$ is negative, and the minimum electric energy occurs when $\theta = \pi/2$. As shown in Eq. (2), the electric force does not directly influence the azimuthal orientation of the director.

The minimum free energy can be found by solving the Euler-Lagrange equations for the total integration of both the elastic and the electric free energy over all liquid crystals. We used a commercially available TECHWIZ 3D software (SANAYI system Co., Ltd., Korea) to calculate the director field. [15] The LC director calculation in TECHWIZ 3D is based on

TABLE I. LC material parameter used in the simulations.

Electrical /optical		Mechanical properties	
n_e	1.586	γ	124 mPa s
n_o	1.483	K_{11}[a]	13.6 pN
$\varepsilon_\parallel$	3.3	K_{22}[a]	4.6 pN
$\varepsilon_\perp$	6.6	K_{33}[a]	14.1 pN
Voltage	7 V	Cell gap	3.2 μm

[a]Elastic constants are variables in each simulation.

Eriksen-Leslie theory, and its accuracy has been confirmed in many papers [16–18]. The material parameters used for the simulation are summarized in Table I where the reference material parameters were obtained from an LC mixture used in commercial LCDs.

Figure 2 shows the results of the first simulation where $K_{11} = K_{33} = 14$ and $K_{22} = 4.6$. As shown in Fig. 2(a), the

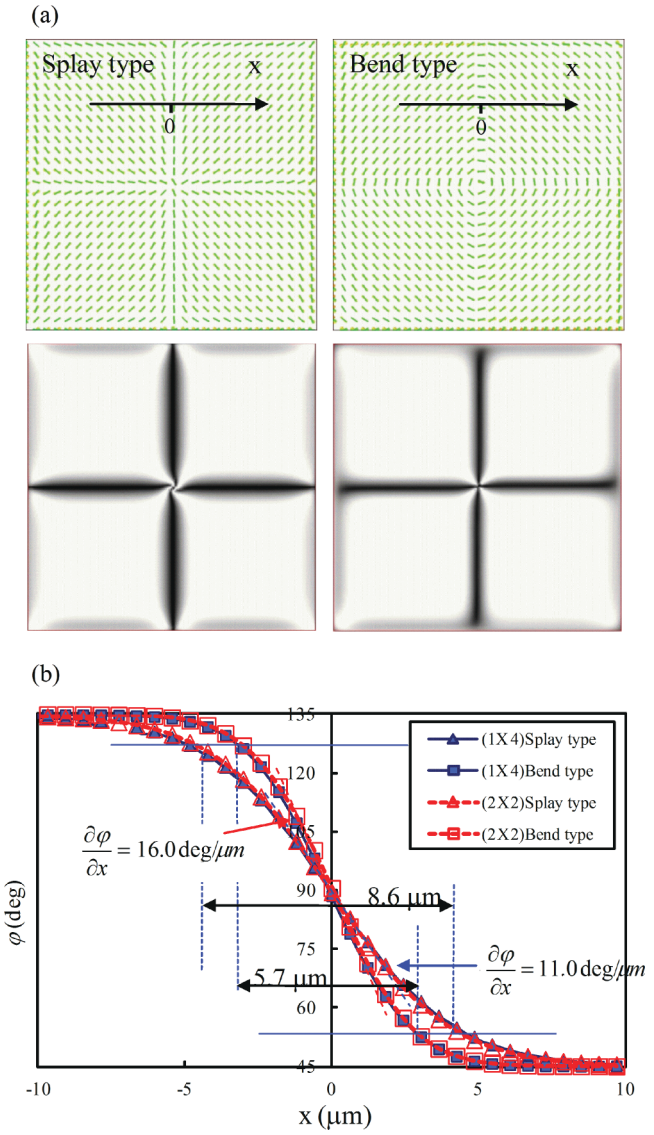

FIG. 2. (Color online) (a) Left: simulations of the bend disclination and right: splay deformation and (b) the azimuthal angle with the x position. In the simulations, $K_{11} = K_{33} = 14$ and $K_{22} = 4.6$.

TABLE II. The slope $(\partial\varphi/\partial x)$ of the azimuthal angle with the x position under various elastic conditions.

	K_{11}	14	14	14	10	18
	K_{33}	14	10	18	14	14
$\partial\varphi/\partial x$	Splay	11.0	11.4	10.8	12.3	10.1
	Bend	16.0	17.9	14.7	16.2	15.9

domain boundary width of the splay type domain is larger than that of the bend type. Figure 2(b) shows the azimuthal angle with the x position in the middle LC layer. Interestingly, the difference between the (1×4) and (2×2) types is only barely observed as shown in Fig. 2(b). The mechanism of the domain boundary formation is quite similar in the two splay types of the (1×4) and (2×2) domains and in the two bend types. In this paper, we consider only the (2×2) domains hereafter, considering that the (2×2) domain is widely used in the photoalignment method.

In Fig. 2(b), the azimuthal deformation $(\partial\varphi/\partial x)$ at the center of domain and the width between azimuthal angles of the director of 54° and 126° (10% to 90%) are indicated in the insets. The domain width for the splay type (8.6 μm) was about 50% larger than that of the bend type (5.7 μm), and the $\partial\varphi/\partial x$ obtained for the splay type was much gentler than that of the bend type. Since the splay and bend elastic constants were set to be same in the simulation, the domain boundary widths were expected to be the same in the two types of domains. Hence, the large difference between the disclination widths of the two types was a quite surprising result.

In order to make the situation clear, we carried out simulations under various elastic constants, and the results are shown in Table II and Fig. 3. Surprisingly, the azimuthal deformations $(\partial\varphi/\partial x)$ of the bend disclinations were always larger than those of the splay disclinations regardless of the values of K_{11} and K_{33} within the range of 10–18. From Fig. 3, we can see that K_{11} mostly influenced the width of the splay type, and K_{33} mostly influenced the width of the bend type as expected. However, even when $K_{11} = 14$ and $K_{33} = 18$, the splay disclination line is wider, and $\partial\varphi/\partial x$ is lower. In this way, the difference between the two domain types is significantly large compared to the influence of the material parameters, such as the bend and splay elastic constants.

III. ANALYSIS AND DISCUSSION

A. Elastic deformation analysis for the splay and bend type domains

We defined the coordinate system, as shown in the inset in Fig. 1(a-ii) in order to investigate the director deformation along the cross-sectional plane A-A'. Since the deformation along the y axis becomes zero, the splay, twist, and the bend deformations can be expressed as follows:

$$\text{div } \mathbf{n} = \left(\frac{\partial n_x}{\partial x}\right) + \left(\frac{\partial n_z}{\partial z}\right), \tag{3}$$

$$\mathbf{n} \cdot \text{curl } \mathbf{n} = \left(n_z \frac{\partial n_y}{\partial x} - n_y \frac{\partial n_z}{\partial x}\right) + \left(n_y \frac{\partial n_x}{\partial z} - n_x \frac{\partial n_y}{\partial z}\right), \tag{4}$$

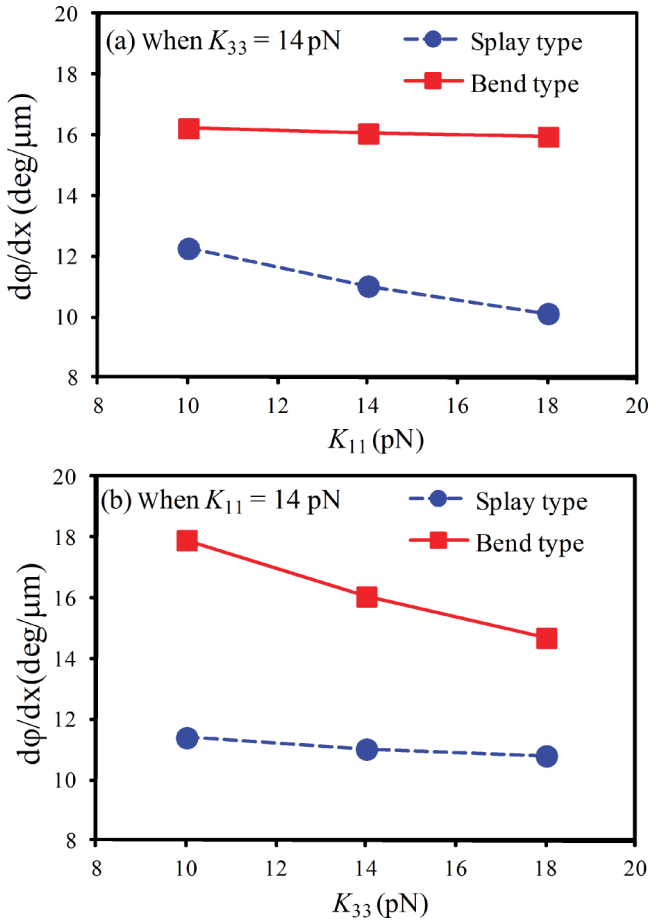

FIG. 3. (Color online) The azimuthal deformation obtained under various elastic conditions of the LC layer.

$$\mathbf{n}\times\text{curl}\,\mathbf{n} = \left[\left(n_y\frac{\partial n_y}{\partial x}+n_z\frac{\partial n_z}{\partial x}\right)\mathbf{i}-n_x\frac{\partial n_y}{\partial x}\mathbf{j}-n_x\frac{\partial n_z}{\partial x}\mathbf{k}\right] + \left[-n_z\frac{\partial n_x}{\partial z}\mathbf{i}-n_z\frac{\partial n_y}{\partial z}\mathbf{j}+\left(n_x\frac{\partial n_x}{\partial z}+n_y\frac{\partial n_y}{\partial z}\right)\mathbf{k}\right]. \quad (5)$$

Here, each deformation can be divided into two deformation components along the x and z directions, which are associated with $\partial/\partial x$ and $\partial/\partial z$, respectively. The first term on the right hand side of Eq. (3) expresses the splay deformation strain along the x direction, which provides a stress on the domain boundary to expand. The second term is the splay strain along the z direction sustaining the electric force. The first and second terms on the right hand side of Eq. (4) are the twist strains along the x and z directions, respectively. While the twist strain along the x axis influences the polar angle of the directors, the twist strain along the z axis influences the azimuthal angle of the director. Hence, the twist strain along the z axis is the main force to determine the azimuthal angle of the directors, which means that the twist strain along the z direction is likely to reduce the domain boundary width. The first and second square brackets on the right hand side of Eq. (5) represent the bend strains along the x and z directions, respectively. Similar to the splay strain, the bend strain along the x direction provides horizontal stress to expand the domain boundary width, whereas, the bend strain along the

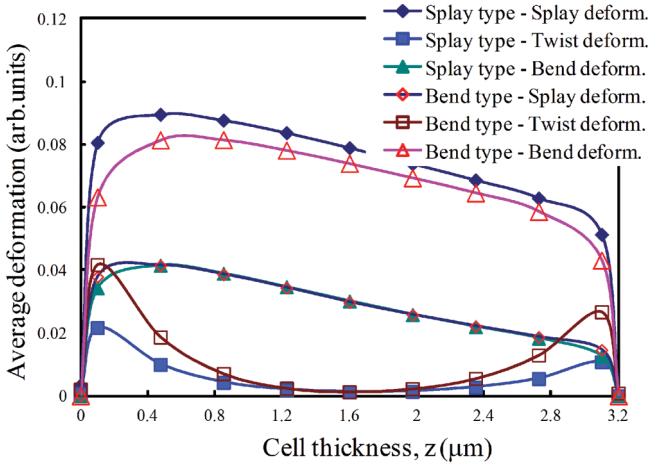

FIG. 4. (Color online) Deformation strain along the x axis, representing components associated with $\partial/\partial x$.

z direction competes with the electrical force. The elastic free energy density [Eq. (1)] is a function of the square of each deformation, and therefore, the elastic free energy of each deformation has three terms, including two terms related to the deformations along the x and z directions and the coupled term of the two deformations. Thus, the coupling strain between the deformations along the x and z axes exists in each deformation [Eqs. (3)–(5)] in addition to the strains along the two axes as described above. In this way, by analyzing each strain component separately, we can easily determine the mechanism regarding the domain boundary width.

By using the director field obtained by simulation with $K_{11} = K_{33} = 14$, the director deformation strains in Eqs. (3)–(5) were calculated numerically. The total sum of the deformation strains along the horizontal direction in the bend type is somewhat larger than that in the splay type due to the narrower domain boundaries, whereas, the total sum along the cell thickness direction is the same in the two types of domains. The difference makes it difficult to fairly compare the two deformations. Hence, the total sum of the strains along the x direction in each type was set to unity so that the horizontal strains can be compared reasonably in Fig. 4, which shows the average deformation strains along the x direction associated with $\partial/\partial x$. The horizontal axis in Fig. 4 is the position along the cell thickness (z), and the vertical axis is the average deformation strains of the LCs at the same z position. Figure 5 shows the deformation strains along the z direction associated with $\partial/\partial z$.

As shown in Fig. 4, in the splay type domains (filled data sets), the splay strain was the largest, the bend strain was in the middle, and the twist strain was the weakest among the x directional deformation strains. On the other hand, in the bend type domains (open data sets), the order of the strength of the splay and bend strains was reversed compared to the splay type. Thus, we can see that the splay deformation is the dominant factor for expanding the domain boundary width in the splay type, and the bend deformation is the dominant factor in the bend type. Meanwhile, the deformation strains near the bottom substrate were larger than those of the other side. This is due to the fact that the boundary between two slanted UV irradiation exists in the bottom substrate as shown in Fig. 1,

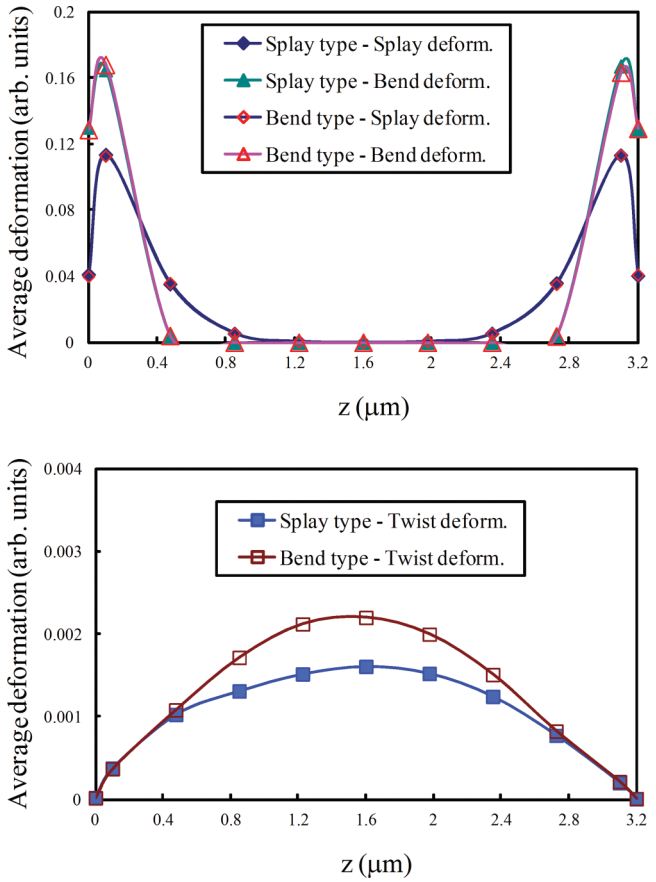

FIG. 5. (Color online) Deformation strain along the z axis, representing components associated with $\partial/\partial z$.

and the horizontal deformation near the bottom substrate is larger than that near the upper substrate.

Interestingly, the twist deformation of the bend type is almost two times larger than that of the splay type, especially near the surfaces in Fig. 4. Due to the larger portion of the twist deformation in the bend type, the portion of the bend deformation is somewhat smaller than the splay deformation in the splay type. Note that the twist deformation along the x direction does not contribute to expand the width of the domain boundary. Hence, the overall elastic strain to expand the boundary width is larger in the splay type than in the bend type. The mechanism causing the difference may be understood by considering the schematics in Figs. 6(a) and 6(b). Whereas, the splay deformation is dominant near the boundary surface in the splay type, the twist deformation is dominant in the bend type. Figure 6(c) shows the average deformation along the x direction near the surface (z = 0–0.32 μm) in both the splay and the bend types. In the splay type, the splay deformation is dominant near the surface across the domain boundary, whereas, in the bend type, the twist deformation is dominant in the same area.

Meanwhile, the strains along the cell thickness direction are shown in Fig. 5 where the splay and bend deformation strains shown in Fig. 5(a) compete with the electric force and are large near the surfaces due to the large polar angle deformation near the surfaces under the application of fields. These strains are almost the same in both the splay and the bend types.

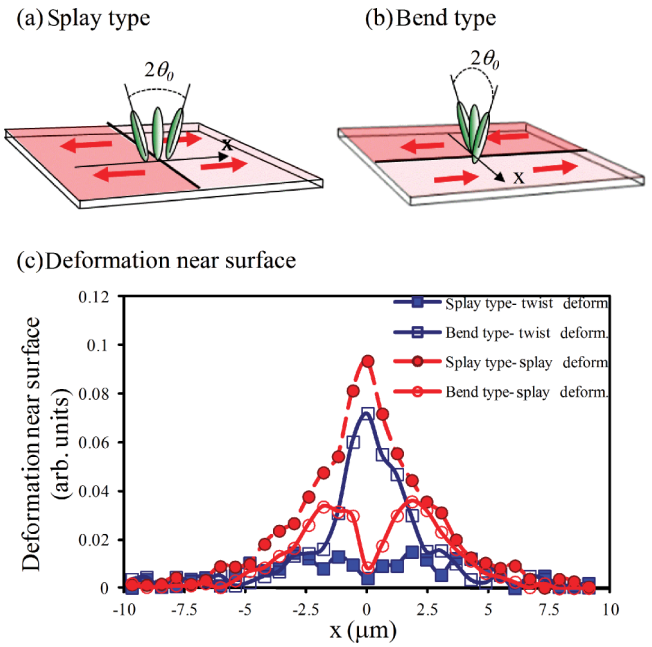

FIG. 6. (Color online) (a) Splay deformation near the surface in the splay type, (b) bend deformation near the surface of the bend type (θ_0: the pretilt angle), and (c) the average deformation near the surface (0–0.32 μm).

Interestingly, a significant difference was found in the twist strain along the z direction between the two types as shown in Fig. 5(b). Note that the twist strain along the z direction sustains the azimuthal alignment in the middle LC layer, and therefore, the stronger the twist strain, the narrower the width of the domain boundary. As a result of the stronger twist strain along the z direction, the bend type domain has a narrower domain boundary. The stronger twist strain is induced by the coupling effect between the twist strains along the x and z axes since the twist strain along the x axis is strong near the surface as shown in Fig. 6(c).

Thus, the large difference between the domain boundary widths of the splay and bend type domains is caused by the deformation difference near the surface. In the bend type domains, the surface induces a rather large twist strain along the x direction, which induces the large twist strain along the z direction. Hence, the force to sustain the domain boundary narrow is large in the bend type domain. By contrast, in the splay type domains, the surface induces splay strain along the x axis, which causes the larger splay strain along the x axis in the middle layer of the LC. Thus, the width of the splay type domain is wider than that of the bend type.

B. The effect of the pretilt angle on the boundary width

The four domains in the photoalignment method are induced by the pretilt angle deviated from the normal to the surface, and therefore, a larger pretilt angle may reduce the width of the domain boundary. In order to confirm this hypothesis, we conducted simulations under various pretilt angle conditions. First, the pretilt angles of the bottom and upper substrates were set at 1.5°, 2.0°, and 2.5° in the simulation, and the azimuthal deformation ($\partial\varphi/\partial x$) along the

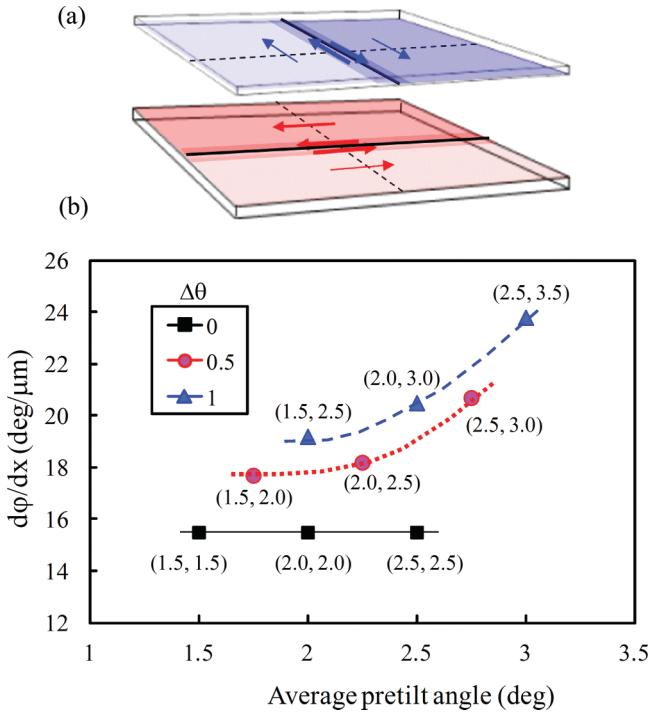

FIG. 7. (Color online) The azimuthal deformation across the domain boundary under various pretilt angle conditions in the bend type domain structure. (θ_1,θ_2) labeled in each point indicates the pretilt angle in the two regions, and the legend indicates the pretilt angle difference.

x axis across the boundary was calculated. The results are shown as the black square data set in Fig. 7. Different from our expectation, $\partial\varphi/\partial x$ was almost independent of the pretilt angle.

In the next simulation, the asymmetric pretilt angle structure shown in Fig. 7(a) was evaluated. In the asymmetric pretilt structure, the pretilt angle near the boundary of the two UV irradiation regions is slightly larger than in the other area. The high pretilt angle region has a width of 5 μm. The pretilt angles (θ_1,θ_2) in the two regions and the difference $(\Delta\theta)$ between the two regions are labeled in each data point and in the legend of Fig. 7(b), respectively. The x axis in Fig. 7(b) is the average pretilt angle of the high and low pretilt angle regions. Surprisingly, the asymmetric pretilt angle increases the $\partial\varphi/\partial x$ value significantly as shown in Fig. 7(b). Moreover, the $\partial\varphi/\partial x$ value further increases with the increasing average pretilt angle. In this way, the adoption of the asymmetric pretilt angle reduces the domain boundary width significantly.

C. Symmetric and asymmetric deformation in the boundary and singular points

Another interesting point is that the luminance profile across the domain boundary is symmetric in the splay type domains, and it is asymmetric in the bend type domains as shown in Figs. 8(a) and 8(b). Figure 8(a) shows the luminance profile where the curve of the splay type exhibits a perfect left-right symmetry, whereas, that of the bend type is slightly shifted to the right side. This effect is also indicated in Fig. 8(b) where the twist deformation along the

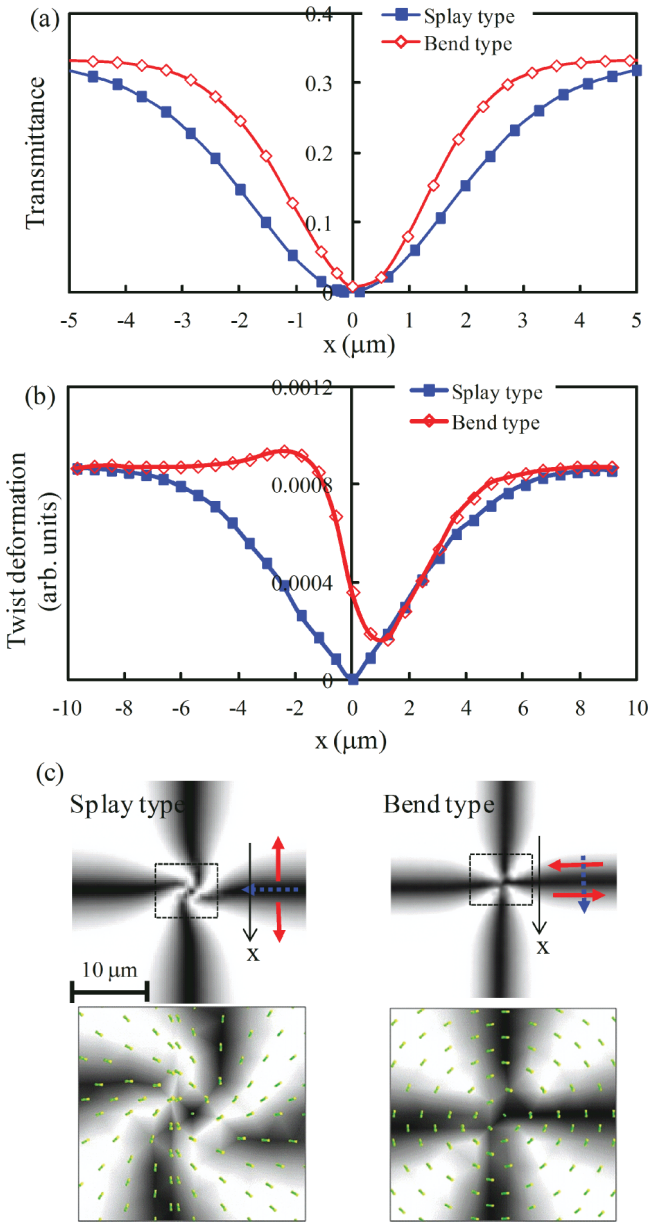

FIG. 8. (Color online) (a) The luminance profile across the domain boundary, (b) the average twist deformation along the z direction $(\partial/\partial z)$, and (c) the two-dimensional luminance near singular points (bottom images are expanded ones with director profiles).

z direction is highly asymmetric in the bend type domains. The reason for this behavior can be understood by analyzing the UV irradiation direction shown in Fig. 8(c) where the red solid lines and dotted blue line represent the UV irradiation directions for the two areas in the bottom and upper substrates, respectively (see Fig. 1). In the splay type, the UV irradiation is perfectly symmetric in the domain boundary, whereas, it is not symmetric in the bend type domains. It produces the asymmetric twist deformation and the asymmetric luminance profile in the bend type domains.

Meanwhile, the +1 defect point in the bend type has a simple cross shape, but the defect point in the splay type has a spiral shape as shown in Fig. 8(c). In the case of the bend type domains, the bend deformation is extended

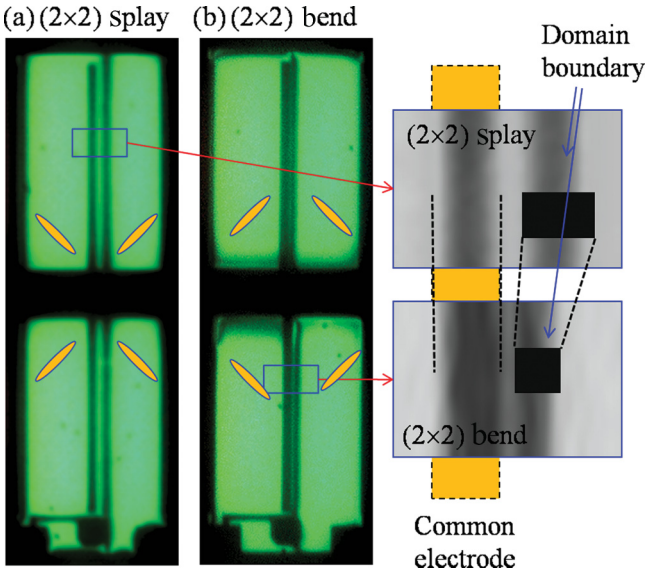

FIG. 9. (Color online) Microscopic photographs of the splay type and bend type domains in a real photoalignment LCD panel. In the two vertical lines in each photograph, the left line is a metal electrode, and the right line is the domain boundary. (Pixel size: 170 × 510 μm.)

to the singular point. However, the splay deformation turns into the bend deformation while approaching the singular point, and as a result, the disclination has a spiral shape near the singular point. It can be understood that the director deformation across the singular point is a twist deformation in the case of the bend type domain, whereas, it is a splay deformation in the splay type domain. The twist deformation requires less deformation energy and is more stable. Hence, the splay type turns into the bend type deformation near the singular point as indicated in the bottom images of Fig. 8(c). The texture difference near the singular points can be reconfirmed by examining the microscopic photographs reported in the references for the splay type domains [15,17] and for the bend type domains. [5]

IV. EXPERIMENTS

The (2 × 2) splay and bend type domains were fabricated in real photoalignment LCD panels by using manufacturing machines at Samsung Electronics Company. However, in the Samsung LCD panel, an opaque common electrode was overlapped with the domain boundaries, which made it difficult to observe the boundaries, as shown in Fig. 9. We found a few panels where the domain boundary and the common electrode were misaligned, and we compared these panels as shown in Figs. 9(a) and 9(b). Although it was not easy to obtain quantitative results due to the common electrode, it was clear that the domain boundary in the bend type domains was thinner than that of the splay type domains as indicated in the right-side insets in Fig. 9.

Comparison of the symmetric pretilt angle and the asymmetric pretilt angle was attempted in another set of real photoalignment panels, which had a different pixel structure from that shown in Fig. 9. The luminance profile was tested by using a Prometric CCD imaging photometer (PM-1433F-1,

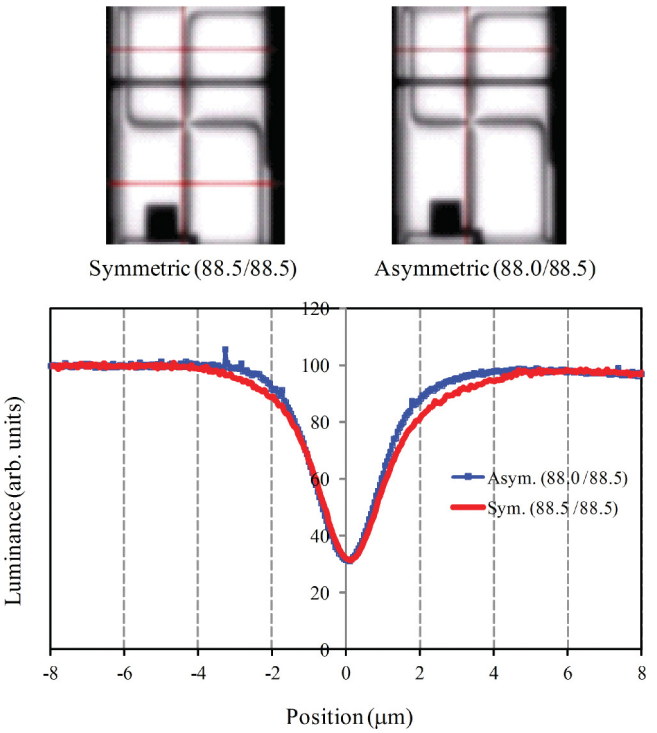

FIG. 10. (Color online) Microscopic images taken by a Prometric CCD imaging photometer for the symmetric and asymmetric pretilt conditions and the luminance as a function of the position across the domain boundary. (Pixel size: 154 × 462 μm; images show a part of the pixel.)

Radiant Imaging, USA). The results demonstrate a clear difference between the two panels as shown in Fig. 10.

V. CONCLUSIONS

We classified the domain boundaries in the multidomain VA LC cells having a right angle director difference between the neighboring domains. The multidomain can be achieved by either (1 × 4) or (2 × 2) area combinations of two substrates. Each method can be classified into splay and bend type domains based on the dominant deformation strain in the boundaries.

Interestingly, in the computer simulations, it was found that the disclination width of the splay type domain was about 50% wider than that of the bend type domain even when the splay and bend elastic constants were the same. The K_{11} and K_{33} constants dominantly influence the width of the splay domain boundary and the bend domain boundary width, respectively, as expected. However, the variation in the boundary width while varying the elastic constants was found to be rather small compared to the difference between the splay and the bend type domains. We analyzed each component of the elastic deformation strains separately in order to investigate the mechanism of the large differences in the domain boundary widths. The large differences were revealed to arise from the different twist deformation strains near the surface, which are significantly larger in the bend type than in the splay type. The large twist deformation along the x direction near the surface in the bend type

domains is coupled with the twist deformation along the z direction in the bulk LCs, causing the stable and narrow domain boundary. Thus, the bulk LC orientation cannot be simply determined only by considering the seeming bulk deformation, but it is basically governed by the surface confinement conditions, such as the pretilt condition, the azimuthal arrangement near the domain boundary, and the surface anchoring.

It was also found that the splay type deformation turned into the bend type deformation near the singular point in order to reduce the deformation energy at the singular point, resulting in a spiral texture. We also suggest an asymmetric pretilt structure, which dramatically reduces the domain boundary width. However, simple adoption of a large pretilt angle is not effective to reduce the width. We compared our simulation results with the experimental results obtained in real LCD panels, and it was confirmed that the experimental results agree qualitatively well with the simulation results.

ACKNOWLEDGMENTS

We thank Samsung Electronics Company for their financial and technical support.

[1] K. Ohmuro, S. Kataoka, T. Sasaki, and Y. Koike, SID Int. Symp. Dig. Tec. **27**, 845 (1997).
[2] K. H. Kim, K. Lee, S. B. Park, J. K. Song, S. N. Kim, and J. H. Souk, *Proceedings of the 18th International Display Research Conference Asia Display, Seoul, Korea, 1998* (Society for Information Display, Campbell, CA, 1998), p. 383.
[3] K. Hanaoka, Y. Nakanishi, Y. Inoue, S. Tanuma, and Y. Koike, SID Int. Symp. Dig. Tec. **35**, 1200 (2004).
[4] M. Schadt, H. Seiberle, and A. Schuster, Nature (London) **381**, 212 (1996).
[5] K. Miyachi, K. Kobayashi, Y. Yamada, and S. Mizushima, SID Int. Symp. Dig. Tec. **41**, 579 (2010).
[6] K. Ichimura, Chem. Rev. **100**, 1847 (2000).
[7] P. K. Son, B. K. Jo, J. C. Kim, T.-H. Yoon, S. J. Rho, S. T. Shin, J. S. Kim, S. K. Lim, and J. H. Souk, Jpn. J. Appl. Phys. **47**, 8476 (2008).
[8] M. Reichenstein, H. Stark, J. Stelzer, and H. R. Trebin, Phys. Rev. E **65**, 011709 (2001).
[9] D. Marenduzzo, E. Orlandini, and J. M. Yeomans, Europhys. Lett. **71**, 604 (2005).
[10] Y. K. Jang *et al*., J. Soc. Inf. Disp. **19**, 253 (2011).
[11] Q. Lin and J.-K. Song, Liq. Cryst. **39**, 333 (2012).
[12] P. G. de Gennes and J. Prost, *The Physics of Liquid Crystals*, 2nd ed. (Oxford University Press, Oxford, 1993), Chap. 4.
[13] J. Nehring and A. Saupe, J. Chem. Phys. **54**, 337 (1971).
[14] F. C. Frank, Discuss. Faraday Soc. **25**, 19 (1958).
[15] H. L. Ong, J. Chou, X. Y. Wang, Y. Qiao, Y. W. Chiu, D. C. Chung, and T. S. Jen, in *Proceedings of the IDW '10, Fukuoka, Japan, 2010* (Society for Information Display, Campbell, CA, 2010), p. 1803.
[16] M. S. Kim, S. M. Seen, and S. H. Lee, Appl. Phys. Lett. **90**, 133513 (2007).
[17] S. H. Lee, S. M. Kim, and S.-T. Wu, J. Soc. Inf. Disp. **17**, 551 (2009).
[18] S. A. Jewell and J. R. Sambles, Appl. Phys. Lett. **84**, 46 (2004).